The *E. coli* NusA carboxy-terminal domains are structurally similar and show specific RNAP- and λN interaction

ANKE EISENMANN, SABINE SCHWARZ, STEFAN PRASCH, KRISTIAN SCHWEIMER, AND PAUL RÖSCH

Department of Biopolymers, University of Bayreuth, 95440 Bayreuth, Germany

Abstract

The carboxy-terminal domain of the transcription factor *Escherichia coli* NusA, NusACTD, interacts with the protein N of bacteriophage λ, λN, and the carboxyl terminus of the *E. coli* RNA polymerase α subunit, αCTD. We solved the solution structure of the unbound NusACTD with high-resolution nuclear magnetic resonance (NMR). Additionally, we investigated the binding sites of λN and αCTD on NusACTD using NMR titrations. The solution structure of NusACTD shows two structurally similar subdomains, NusA(353–416) and NusA(431–490), matching approximately two homologous acidic sequence repeats. Further characterization of NusACTD with ^{15}N NMR relaxation data suggests that the interdomain region is only weakly structured and that the subdomains are not interacting. Both subdomains adopt an $(HhH)_2$ fold. These folds are normally involved in DNA–protein and protein–protein interactions. NMR titration experiments show clear differences of the interactions of these two domains with αCTD and λN, in spite of their structural similarity.

Keywords: NusA; anti-termination; termination; NMR; RNA polymerase; N-protein; phage λ; HhH motif

RNA synthesis in *Escherichia coli* is catalyzed by RNA polymerase (RNAP), a multiprotein enzyme whose core shows an $\alpha_2\beta\beta'$ subunit composition (Nudler 1999). After initiation of transcription, the essential transcription factor NusA (N utilization substance A) associates with the RNAP core enzyme, where it modulates transcriptional pausing, termination, and anti-termination (Liu et al. 1996).

The crystal structures of two non-*E. coli* NusA factors have been solved so far (*Thermotoga maritima* [Worbs et al. 2001; Shin et al. 2003], *Mycobacterium tuberculosis* [Gopal et al. 2001]). These structures show a common domain organization, that is, an amino-terminal RNAP-binding domain, followed by one S1 and two KH (K homology) RNA-binding domains. This NusA core organization is conserved in all bacteria for which such sequence information is available. An additional carboxy-terminal region, NusACTD, comprising ~160 residues is found in several α-, β-, and γ-proteobacteria like the enterobacterium *E. coli*, as well as in *Chlamydia* or *Treponema* (Mah et al. 2000). Though NusACTD is not as highly conserved as the NusA core, the region is characterized by its acidity and frequently by an internal sequence repeat of ~70 residues.

NusACTD probably serves as a multipurpose protein–protein interaction site as suggested by the existence of different binding partners of NusACTD in distinct elongation complexes (Mogridge et al. 1995, 1998; Mooney et al. 1998; Mah et al. 1999, 2000; Gusarov and Nudler 2001; Bonin et al. 2004). In spite of the fact that NusA harbors three RNA-binding domains, the affinity of isolated NusA to RNA is rather weak (Mogridge et al. 1995). Binding studies with deletion mutants of NusA, however, indicate that RNA binding to *E. coli* NusA is hindered by the 80 carboxy-terminal residues of NusACTD (Mah et al. 2000). Furthermore, αCTD counteracts the inhibitory effect of the carboxy-terminal 80 residues by binding to NusACTD, thus providing a model for the regulation of RNA binding in the NusA:RNAP complex in vivo (Mah et al. 2000).
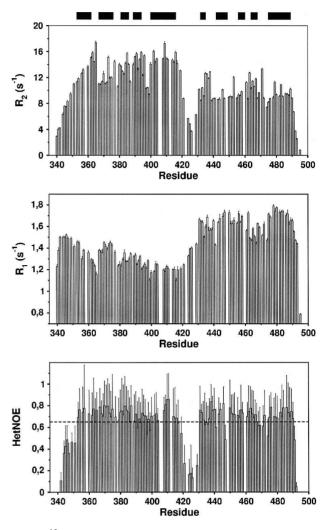
A similar mechanism to enhance the intrinsic RNA-binding capacity of NusA was suggested for the λN protein (Mah et al. 2000), which binds to NusA during λN-mediated anti-termination (for recent reviews, see Gusarov and Nudler 2001 and Nudler and Gottesman 2002). The minimal fragment of λN required for the λN–NusA interaction consists of residues N34–K47 (Mogridge et al. 1998). Recently, Bonin et al. (2004) determined the X-ray structure of the λN(34–40)·NusA(352–421) complex and presented calorimetric data that indicated an interaction of λN(41–47) with NusACTD outside NusA(352–421). However, in contrast to αCTD, λN(34–47) was not able to stimulate RNA binding to NusA (Mogridge et al. 1998; Bonin et al. 2004). Thus, Bonin et al. (2004) inferred a simple scaffold function for NusACTD in the λN:NusA complex, and suggested different binding sites for αCTD and λN on NusA(431–490). A direct interaction between NusA(431–490) and λN(41–47), however, has not been demonstrated yet, and it is not known whether αCTD and λN bind simultaneously to NusACTD in the anti-termination complex.

The modular architecture of the proteins establishing the termination and anti-termination complexes allows dissection and investigation of isolated domains and complexes thereof. We used this fact to determine the three-dimensional solution structure of NusA(339–495) to high resolution, its dynamic properties, and its interaction sites with λN(1–53) and αCTD(233–329) using NMR spectroscopy.

Results and Discussion

Structure calculation and validation

Initial analysis of ^{15}N relaxation data (Fig. 1) revealed significant variations of the $\{^1H\}^{15}N$ heteronuclear NOE (HetNOE) and the relaxation rates along the backbone.

Figure 1. ^{15}N transverse (R_2, *top*) and longitudinal (R_1, *middle*) relaxation rates, and $\{^1H\}^{15}N$ heteronuclear NOE (*bottom*) at 14.1 T. Negative values of the HetNOE for amino- and carboxy-terminal residues (T340, V341, D493, A495) have been omitted for clarity. The black bars represent helices. The evident difference of average R_2 values for residues A350–A420 and residues P430–W490, together with the relatively low values (<0.65; see dotted line) of the HetNOE in between residues A420 and P430 corraborates the existence of two subdomains separated by a mobile linker or hinge region. Quantitative analysis of the relaxation data indicates that the two subdomains reorient partially independent in solution and are noninteracting.

Values of the HetNOE <0.65 at 600 MHz are indicative of a considerable flexibility on a picosecond timescale (Tjandra et al. 1995) and could be observed for the amino- and carboxy-terminal regions of NusACTD as well as residues I417–P430. Higher average values of the HetNOE ~0.7 were found for NusA(353–416) and NusA(431–490), suggesting that these parts of the peptide chain are structured.

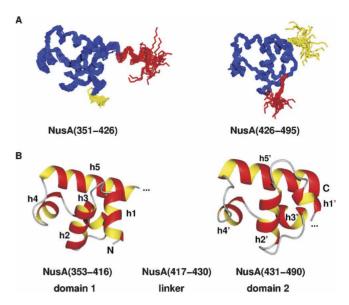Both NusA(353–416) and NusA(431–490) exhibit similar average values of the longitudinal R_1 rates, $1.3 \pm 0.1 \, \text{sec}^{-1}$

and $1.6 \pm 0.9 \ \text{sec}^{-1}$, but show different average transversal R_2 rates, $13.6 \pm 1.9 \ \text{sec}^{-1}$ and $9.9 \pm 1.5 \ \text{sec}^{-1}$, respectively. As the R_2/R_1 ratio for rigid residues is related to the rotational correlation time τ_c (Kay et al. 1989), the different R_2/R_1 ratios of NusA(353–416) and NusA(431–490), together with the low HetNOE values for NusA(417–430), suggest that NusACTD consists of two domains that are separated by a flexible linker region.

The hypothesis of NusACTD exhibiting a two-domain structure is supported by the fact that different ranges of residual dipolar couplings (RDCs) were observed for NusA(353–416), -12.4–19.0 Hz, and for NusA(431–490), -8.3–11.0 Hz, indicating different alignment tensors for these domains (Bax et al. 2001). In fact, in the course of molecular dynamics simulations, the magnitude of the alignment tensor D_a could be determined as 10.5 ± 0.25 Hz [NusA(353–416)] and 6.5 ± 0.25 Hz [NusA(431–490)], while the rhombicities R were 0.2 ± 0.05 for NusA(353–416) and 0.3 ± 0.05 for NusA(431–490). The average alignment of both domains cannot be described by a single alignment tensor; therefore, the significantly different tensor components (Table 1) imply considerable relative motion of NusA(353–416) and NusA(431–490) (Braddock et al. 2001, 2002).

All NOESY cross-peaks could be interpreted as short distances between protons within the domains NusA(353–416) and NusA(431–490), respectively, and no NOE between the two domains could be observed. Therefore, though NMR experiments were performed using the complete NusACTD, structures were calculated separately for NusA(351–426) and NusA(426–495). Residues 339–350 were not included in the structure calculation, as this region lacked nontrivial interresidual NOEs and showed low HetNOE values, indicating high flexibility of the amino terminus.

The structure calculation based on NMR-derived restraints resulted in ensembles with high precision of atomic coordinates for both domains (Fig. 2A). No violations of distance restraints > 0.16 Å, dihedral angle restraints $> 3°$, or RDCs > 0.72 Hz could be observed (Table 2). Further validation of the structures with PROCHECK 3.5.4 (Morris et al. 1992; Laskowski et al. 1993) showed that 92.1% [NusA(351–426)] and 95.3% [NusA(426–495)] of the nonglycine and nonproline residues adopted a con-

Figure 2. Structure of the carboxy-terminal domain of NusA. (*A*) Backbone overlay of the 19 accepted structures for the two subdomains of the carboxy-terminal domain of NusA, NusA(351–426), and NusA(426–495), respectively. The linker residues are shown in red; flexible residues at the amino and carboxyl terminus are depicted in yellow. (*B*) Lowest energy structures of the relatively rigid parts of NusACTD, NusA(353–416), and NusA(431–490) in ribbon representation. Each subdomain contains two HhH motifs that are linked together by a so-called connector helix, thus adopting a compact $(\text{HhH})_2$ fold. Helices h1/h1′ and h2/h2′ constitute the first and h4/h4′ and h5/h5′ the second HhH motif, whereas h3/h3′ represent the connector helices. The linker between the two subdomains seems to be structured (see *A*, red part of overlay); however, ^{15}N relaxation data indicate that the interdomain region comprising about 14 amino acids is flexible. The picture was drawn with MOLMOL (Koradi et al. 1996).

formation within the most favored regions of the Ramachandran plot.

The solution structures of NusA(351–426) and NusA(426–495) were deposited in the Protein Data Bank (PDB) (Berman et al. 2000), accession codes 1WCL and 1WCN.

Structure of NusACTD

NusACTD consists of two subdomains, NusA(353–416) and NusA(431–490), that are connected by a linker region (Fig. 2B). Either subdomain contains two helix-hairpin-

Table 1. *Alignment data for NusA(353–416) and NusA(431–490)*

	D_a (Hz)	R	A_{zz} (Hz)	A_{yy} (Hz)	A_{xx} (Hz)
NusA(353–416)	10.25 ± 0.25	0.20 ± 0.05	20.50 ± 0.50	-13.65 ± 1.11	-7.35 ± 0.96
NusA(431–490)	6.25 ± 0.25	0.30 ± 0.05	12.50 ± 0.50	-9.43 ± 0.85	-3.85 ± 0.63

Shown are the magnitude of the alignment tensor D_a and the rhombicity R, as well as the eigenvalues of the alignment tensor A_{zz}, A_{yy}, and A_{xx}. Different alignment tensors for individual domains indicate the presence of medium- to large-scale interdomain motions (Braddock et al. 2001).

Table 2. *Summary of the structure calculation of NusA(351–426) and NusA(426–495)*

Experimental restraints used for the structure calculation		NusA(351–426)	NusA(426–495)
Distance restraints	Total	883	699
	Sequential	328	285
	Medium-range	278	191
	Long-range	268	199
	Ambiguous/intramol.	9	24
Dihedral angles		39	28
Dipolar couplings		37	32
Hydrogen bonds (2 restraints each)		19	20
Molecular dynamics statistics			
Energies (kcal/mol)			
	E_{pot}	23.1324 ± 1.7314	17.4150 ± 1.1643
	E_{bond}	1.0164 ± 0.0879	0.8981 ± 0.0962
	E_{angle}	8.7168 ± 0.8408	6.5624 ± 0.6648
	E_{impr}	2.6457 ± 0.2801	1.6269 ± 0.2001
	E_{vdW}	5.2270 ± 1.0387	2.8016 ± 0.6186
	E_{NOE}	4.0465 ± 0.5038	3.4700 ± 0.5815
	E_{edih}	0.0322 ± 0.0495	0.0752 ± 0.0846
	E_{sani}	1.4478 ± 0.4740	1.9808 ± 0.4104
RMSDs from ideal distances (Å)	Bond lengths	0.0007 ± 0.0001	0.0009 ± 0.0001
	Distance restraints	0.0054 ± 0.0004	0.0097 ± 0.0008
RMSDs from ideal angles (deg)	Bond angles	0.1169 ± 0.0065	0.1520 ± 0.0075
	Dihedral angle restraints	0.0655 ± 0.0303	0.3179 ± 0.2822
RMSDs from dipolar couplings (Hz)		0.1978 ± 0.0327	0.2488 ± 0.0249
Atomic RMSDs of structural ensemble (Å)			
Backbone heavy atoms[a]		0.34 (H353–T416)[b]	0.36 (A431–W490)[b]
Heavy atoms[a]		0.70 (H353–T416)[b]	0.72 (A431–W490)[b]
Ramachandran Plot statistics			
Residues in			
	Most favored regions	92.1%	95.3%
	Allowed regions	7.0%	4.4%

Except for the experimental restraints and the atomic RMSD data, all values are average values over the 19 accepted structures in the format average value ± standard deviation.
[a] Structural precision was calculated with reference to the structure with lowest value of the target function.
[b] All residues were included for calculation of the structural superposition.

helix (HhH) motifs, each formed by two anti-parallel α-helices connected by a short hairpin (Doherty et al. 1996).

The amino-terminal HhH motif of NusA(353–416), HhH1, is composed of helices h1 (H353–Y362) and h2 (E367–E376) and interacts with the carboxy-terminal HhH motif of the first domain, HhH2, constituted by helices h4 (M389–E394) and h5 (E400–T416). Analogously, the amino-terminal HhH motif of NusA(431–490), HhH1′, which comprises helices h1′ (D432–L435) and h2′ (R442–A449), packs on the carboxy-terminal HhH motif, HhH2′, which includes helices h4′ (I464–A468) and h5′ (D475–C489).

The interhelical angles of the HhH motifs range from 119° to 129° (HhH1, 119°; HhH2, 124°; HhH1′, 129°; HhH2′, 122°), slightly less than the interhelical angles of 130°–155° described for HhH motifs earlier (Doherty et al. 1996; Shao and Grishin 2000). These deviations from canonical HhH

motifs can be interpreted in the context of the observed flexibility and the small database used for the determination of the interhelical angles in Doherty et al. (1996).

The tight packing of the two HhH motifs results in the formation of a compact hydrophobic core, which is completed by the helix connecting the two HhH motifs in each subdomain, helix h3 (L381–Y386) and helix h3′ (L456–A460). This arrangement of two HhH motifs linked by a connector helix has been classified as a separate fold termed (HhH)$_2$ (Shao and Grishin 2000).

(HhH)$_2$ folds are mainly implicated in DNA binding (Shao and Grishin 2000), as confirmed by a search of the PDB (Berman et al. 2000) using the average structures of NusA(353–416) and NusA(431–490) with the DALI program (Holm and Sander 1996). However, both domains show similarity to the SAM (sterile <u>α</u> <u>m</u>otif) domain of

the ephrin 2 receptor (PDB 1b4f; Thanos et al. 1999). This is a typical representative of proteins whose $(HhH)_2$ fold mediates protein–protein interactions.

Comparison of the two subdomains of NusACTD

Overlay of the average structures of NusA(356–415) and NusA(431–490) results in a backbone RMSD of 1.9 Å, and thus confirms that the sequence homology of the acidic repeats is reflected in the three-dimensional structure. The superposition of the two domains (Fig. 3) shows similar positions and orientations for helices h2–h5 and h2′–h5′, but not for helices h1 and h1′, though all helices tend to be shorter in the second domain.
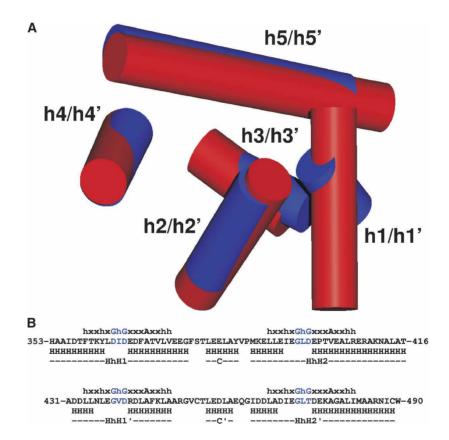
Both domains are considerably acidic with net charges of $-11e^-$ and $-9e^-$ and theoretical pIs of about 4. The two domains show clear differences in the distribution of polar and hydrophobic as well as charged residues (Fig. 4), which may explain their differential recognition of binding partners.
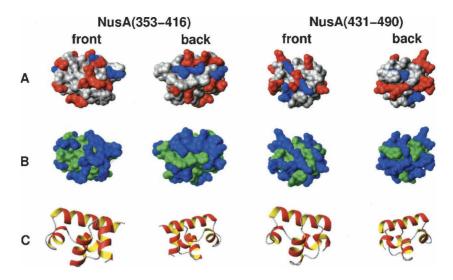
Oligomeric state of NusACTD

$(HhH)_2$ motifs have been implicated in oligomerization (Kim and Bowie 2003), which would have to be considered in the analysis of relaxation data.

To examine the possible formation of oligomers, we performed translational diffusion measurements (Wilkins et al. 1999) at concentrations of 0.175, 0.35, and 0.70 mM NusACTD. The resulting average hydrodynamic radius of $r_H = 25.5 \pm 0.3$ Å was found to be independent of the protein concentration, which clearly indicates the virtual

Figure 3. The sequence homology of the two subdomains in the carboxy-terminal part of NusA is mirrored in the structural similarity of NusA(353–416) and NusA(431–490). (*A*) Overlay of NusA(353–416) and NusA(431–490). The arrangement of helices [NusA(353–416), h1–h5; NusA(431–490), h1′–h5′], which are represented as red and blue cylinders for NusA(353–416) and NusA(431–490), respectively, reveals a common overall fold. In contrast to helices h1 and h1′, helices h2–h5 share similar positions and orientations with h2′–h5′, though helices in the second subdomain tend to be shorter. The superposition was calculated for the backbone atoms of I356–A415 and A431–W490 and drawn using MOLMOL (Koradi et al. 1996). (*B*) Alignment of NusA(353–416) and NusA(431–490) with T-Coffee (Notredame et al. 2000) shows a sequence identity and homology of 31.3% and 60.9%, respectively. The secondary structure (H, helix), the helix-hairpin-helix (HhH) motifs as well as the connector helix (C) are reported beneath the sequence with primes for the second subdomain. For comparison, the 16-residue sequence characteristic of HhH motifs (Doherty et al. 1996) is shown *above* the sequence and the Gly—hydrophobic amino acid—Gly (GhG) pattern in the hairpin is highlighted in blue. Note that in all HhH motifs occuring in NusACTD, the second Gly that serves as a helix cap (Doherty et al. 1996) is replaced by more typical helix-capping residues like Asp or Thr (Kumar and Bansal 1998).

Figure 4. Surface representations of the lowest energy structures of NusA(353–416) and NusA(431–490) showing the distribution of charged (*A*) and polar residues (*B*). As a reference, the corresponding orientations of the subdomains are drawn in ribbon style (*C*). Both charged (negative, red; positive, blue; neutral, gray) and polar (polar, blue; hydrophobic, green) residues are differently distributed on the surface. The preparation of the figure was done using MOLMOL (Koradi et al. 1996).

absence of a fast monomer–oligomer equilibrium in the protein solution. In addition, the value of r_H cannot be explained in terms of dimer or higher oligomer formation of NusACTD. Although the hydrodynamic radius of a hypothetical spherical NusACTD can be estimated to be 20.7 Å for a monomer and 25.3 Å for a dimer (Wilkins et al. 1999), a more realistic calculation with an elongated NusA(353–490) structure using a shell model (de la Torre and Carrasco 2000) leads to a hydrodynamic radius of 22.7 Å. The difference between this value and the experimental value of 25.5 Å may easily be explained by the fact that the flexible amino- and carboxy-terminal residues could not be taken into account in this model. Thus, the experimental value for the hydrodynamic radius is virtually identical to the one calculated from a monomer model.

Rotational diffusion of NusACTD

[15]N relaxation data of anisotropically tumbling proteins contain information about the orientation of each N-H[N] vector relative to the overall diffusion frame of the molecule. Therefore, this data is frequently used to determine the relative orientation of individual domains in multidomain proteins (for review, see Fushman et al. 2004). This approach, however, assumes domains with fixed relative orientations. In all other cases, the diffusion of the domains will not only be governed by the diffusion of the particle as a whole, but will be influenced to a certain extent by the diffusional properties of the single domains. Thus, by calculating the diffusion tensor separately for each domain within a multidomain protein, it is pos-

sible to determine whether the domains are mutually independent.

This is clearly the case for NusA(353–416) and NusA(431–490). Quantitative analysis of the ^{15}N data reveals significantly different diffusion tensors for these domains (Table 3), leading to the conclusion that their movements are highly uncorrelated.

The rotational correlation times were calculated from the ^{15}N relaxation rates R_1 and R_2 that were determined for residues inside NusA(353–416) and NusA(431–490) in the intact NusACTD. The resulting correlation times were 9.5 ± 0.3 nsec and 7.0 ± 0.2 nsec, respectively, both values being higher than the roughly 4.5 nsec expected for globular, compact proteins of 64 and 60 residues (Maciejewski et al. 2000). This difference, however, may easily be explained by the fact that unstructured regions precede and follow the two domains of NusACTD, and that these domains are connected by a linker. The linker and the terminal extensions affect the rotational correlation times of the isolated domains in different ways. First, the linker restricts the relative movements of the two domains, which leads to an increase in the tumbling times of NusA(353–416) and NusA(431–490). Second, flexible termini can enhance the rotational correlation times significantly (Tjandra et al. 1995), which is reflected in the tumbling time of NusA(353–416) compared with NusA(431–495).

Taken together, the alignment and relaxation data strongly suggest that NusA(353–416) and NusA(431–490) are not interacting or are preferentially orientated relative to each other. This justifies our initial approach to treat the domains separately.

Table 3. *Diffusion tensor analysis from R_2 and R_1 data at 600 MHz of NusA(353–416) and NusA(431–490)*

Diffusion tensor statistics[a]

	Isotropic		Axially symmetric (prolate)		Axially symmetric (oblate)		Anisotropic	
	$\chi^2_{(5\%)}$	χ^2_{exp}	$\chi^2_{(5\%)}$	χ^2_{exp}	$\chi^2_{(5\%)}$	χ^2_{exp}	$\chi^2_{(5\%)}$	χ^2_{exp}
NusA(353–416)	44.2	207.6	40.0	48.5	39.7	48.5	37.0	19.0
NusA(431–490)	31.4	55.98	26.6	24.3	28.0	39.7	23.4	22.9

Diffusion tensor components[b]

	D_{zz} $(10^7\ s^{-1})$	D_{yy} $(10^7\ s^{-1})$	D_{xx} $(10^7\ s^{-1})$	ζ	η	$\tau_{c,eff}$ [ns]
NusA(353–416)	2.31 ± 0.05	1.73 ± 0.06	1.22 ± 0.05	1.6 ± 0.1	0.91 ± 0.19	9.5 ± 0.3
NusA(431–490)	3.11 ± 0.12	2.01 ± 0.07	2.01 ± 0.07	1.6 ± 0.1	0	7.0 ± 0.2

[a] $\chi^2_{(5\%)}$ corresponds to the $\alpha = 0.05$ confidence limit for the fit derived from 500 Monte Carlo simulations, χ^2_{exp} refers to the value of the target function used for the fit. Values of $\chi^2_{(5\%)}$ and χ^2_{exp} for accepted models are shown in bold italic. An F-statistic was used to differentiate between the prolate (four parameters) and the fully asymmetric model (six parameters) for NusA(431–490). The critical values for the F-statistic with $\alpha = 0.1$ amount to $F_{exp} = 4.6$ and $F_{(10\%)} = 22.3$, indicating that the improvement of the fit upon using the six-parameter model is not statistically relevant (Mandel et al. 1995; Dosset et al. 2000). NusA(431–490) is thus best described by a prolate axially symmetric diffusion model, NusA(353–416) by an anisotropic diffusion tensor.
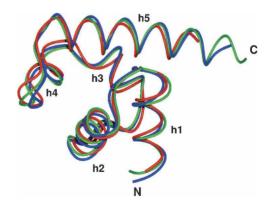
[b] Diffusion tensor components from R_2 and R_1 data at 600 MHz [NusA(353–416): 33 N-H^N vectors; NusA(431–490): 21 N-H^N vectors] for accepted models of NusA(353–416) and NusA(431–490). For a prolate diffusion tensor $(D_{zz} - D_{yy} \geq D_{yy} - D_{xx})$ the anisotropy and rhombicity are defined as $\zeta = 2D_{zz}/(D_{xx} + D_{yy})$ and $\eta = 3/2 \cdot (D_{yy} - D_{xx})/D_{zz} \cdot \zeta/(\zeta - 1)$, respectively, and characterize the deviations from a spherical top (Fushman et al. 2004). The effective rotational correlation time is related to the diffusion tensor components via $\tau_{c,eff} = 1/(2D_{xx} + 2D_{yy} + 2D_{zz})$. Parameter uncertainties of the diffusion parameters were taken from 500 Monte Carlo simulations.

Comparison of free and complexed NusACTD

Recently, the structure of the complex of λN(34–47) with two fragments of NusA, NusA(352–419), and NusA(352–421), respectively, has been determined by X-ray crystallography (Bonin et al. 2004). The NusA molecules are crystallographically independent, but structurally similar with an RMSD of the backbone heavy atoms of 0.67 Å for H353–T416. Both structures deviate only slightly from the uncomplexed solution structure of NusA(353–416), with an RMSD of the backbone heavy atoms of 1.20 Å and 1.10 Å (Fig. 5). Only minor differences between the free and the complexed structures could be observed, and most of these differences are located in the amino-terminal helix and the hairpin of the second HhH motif, involving M389–D399. These residues feature decreased HetNOE values in the free NusACTD, reflecting increased flexibility on a pico- to nanosecond time scale. λN(34–47) contacts this region via L40 by side-chain–side-chain interactions with L398, supporting the idea that the flexibility of the helix and the adjacent hairpin might play an important role in recognition (Atkinson and Kieffer 2004). Thus, in general, conformational rearrangements upon complex formation are minor, in line with the suggested function of NusA(353–416) as a scaffold conferring additional stability to the complex (Bonin et al. 2004).

Interactions of NusACTD with αCTD and λN

In order to elucidate the sites of NusACTD that bind λN and αCTD, ^{15}N-labeled NusACTD was titrated
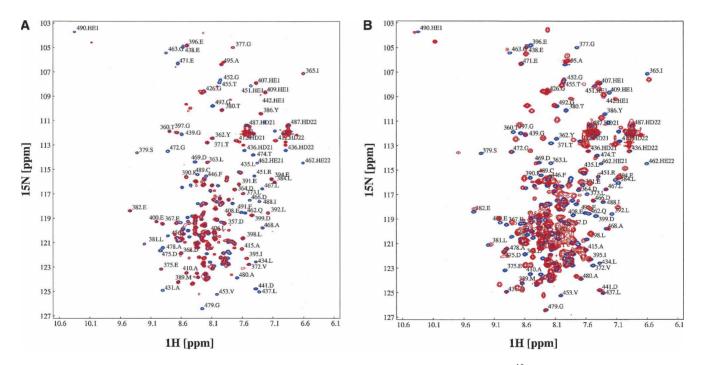

Figure 5. Overlay of the uncomplexed average structure of NusA(353–416) solved by NMR (this work, red) with the crystal structure 1U9L (Bonin et al. 2004), in which NusA(352–419) (chain A in 1U9L, blue) and NusA(352–421) (chain B in 1U9L, green) form a complex with λN(34–47), respectively. Chains A and B are crystallographically independent, but almost identical to each other with an RMSD of the backbone heavy atoms of 0.67 over residues H353–T416. Both structures deviate only slightly from the uncomplexed NusA(353–416), with a backbone RMSD of 1.20 and 1.10, for chains A and B, respectively. The overlay was calculated and drawn with MOLMOL.

with unlabeled αCTD or unlabeled λN(1–53). HSQC spectra of the sample were taken after each titration step (Fig. 6).

Line broadening or chemical-shift changes could be observed for approximately two-thirds of the resonances of NusACTD throughout the titration with λN(1–53), beginning with a NusACTD:λN(1–53) ratio of 0.4 and ending with a ratio of 3.4. Most resonances were broadened beyond detection starting from a NusACTD:λN(1–53) ratio of 1.3 and thus could not be tracked during the titration. From a ratio of 2.6, resonances appeared at new positions in the spectra, probably from the NusACTD:λN(1–53) complex. This broadening and reappearance of resonances is typical for intermediate exchange processes (Zuiderweg 2002) and prevented detection of resonances for a wide range of concentration ratios.

During the titration, 98% and 70%, respectively, of the assigned backbone amide cross-peaks in the first and second domain showed significant changes in resonance intensity or position (≥ 0.05 ppm in ^{1}H or ≥ 0.4 ppm in ^{15}N dimension). As most residues were affected by the presence of λN(1–53), it was impossible to delineate a contact interface of λN(1–53) on NusACTD. Widespread chemical-shift perturbations may indicate allosteric processes (Stevens et al. 2001). Comparison of the free and complexed NusA(353–416), however, clearly shows that the first domain of NusACTD does not undergo major rearrangements upon complex formation. Although no complex structure is available for the second domain of NusACTD, λN is believed to bind in a similar fashion to both domains (Bonin et al. 2004), rendering large-scale structural changes unlikely. Instead, the scattered chemical-shift perturbations might be explained by subtle changes in the tertiary structure. Nevertheless, given that λN(1–53) and NusACTD are strongly oppositely charged, unspecific interactions cannot be ruled out. In summary, both domains of NusACTD are affected by the presence of λN(1–53), providing direct evidence for an interaction of λN(1–53) with NusA(353–416) and NusA(431–490).

Addition of αCTD to ^{15}N-labeled NusACTD resulted in changes in HSQC resonance intensity or position for approximately one-third of the total NusA(339–495) backbone amide resonances from the first titration step (NusACTD:αCTD ratio of 0.5). Most of the perturbed resonances exhibited severe line broadening above a NusACTD:αCTD ratio of 1.1, and thus, could not be followed during the titration. Some of the affected resonances remained visible at all examined NusACTD:

Figure 6. Titration of NusACTD with αCTD and λN(1–53). (*A*) Interaction of NusACTD with αCTD. ^{15}N-labeled GP-NusA(339–495) was titrated with unlabeled αCTD until no further changes were observed in the spectra, resulting in a NusACTD:αCTD ratio of 1:2.1. Shown are the overlays of the ^{1}H^{15}N-HSQC spectra at 700 MHz of the end points of the titrations, corresponding to the free (blue) and complexed (red) NusACTD. (*B*) Interaction of NusACTD with λN(1–53). ^{15}N-labeled GP-NusA(339–495) was titrated with λN(1–53) until no further changes were observed in the spectra, resulting in a NusACTD:λN(1–53) ratio of 1:3.4. Shown are the overlays of the ^{1}H^{15}N-HSQC spectra at 700 MHz of the end points of the titrations, corresponding to the free (blue) and complexed (red) NusACTD.

αCTD ratios up to the end point of the titration (NusACTD:αCTD ratio of 2.1), again indicating intermediate exchange rather than protein aggregation.

In total, chemical-shift changes could be observed for 98% of the resolved backbone amide resonances of the second domain, respectively, whereas the resonances in the first domain remained unaffected by the presence of αCTD. Though no defined contact interface of αCTD on NusACTD could be derived by the titration experiments, the data clearly argue for αCTD binding solely to NusA(431–490). Together with structural data and the fact that αCTD is able to relieve the inhibitory effect of NusACTD on RNA binding (Mah et al. 2000), the titration data strongly suggest that NusA(431–490) functions as a domain regulating RNA binding.

Implications for the role of NusACTD in termination and anti-termination

In summary, the structural data provided here suggests how NusACTD functions as a versatile protein–protein interaction site in different transcription complexes. The domain structure offers an explanation of how NusA(431–490) regulates RNA binding to NusA. The flexible linker allows rearrangement of NusA(431–490) relative to the rest of the protein to facilitate access to the RNA-binding sites of NusA on complexation with αCTD. Spatial adaptability might also play a role in switching from the termination-competent NusA:RNAP complex to the λN:NusA:RNAP complex, which is capable of anti-termination.

In addition to its regulatory function, the NusA(431–490):αCTD interaction possibly enhances the stability of the NusA:RNAP complex (Liu et al. 1996). This could explain why a mutant NusA with residues L344–A495 missing prevents bacterial growth at elevated temperatures (Tsugawa et al. 1988).

We demonstrated in NMR-titration experiments that λN(1–53) binds to both domains of NusACTD, NusA(353–416), and NusA(431–490). The region responsible for the NusACTD interaction on λN is presumably located within residues N34–K47 (Mogridge et al. 1998). Despite its probable binding to NusA(431–490), λN(34–47) cannot stimulate NusA's intrinsic RNA-binding capacity (Bonin et al. 2004). NusA, however, does bind sequence specifically to *nut* RNA in λN:NusA:*nut* complexes (Mogridge et al. 1995; Mah et al. 2000). The K_D of full-length λN and NusA or a λN:*nutBoxB*:NusA complex is of the order of 50 nM (van Gilst and von Hippel 1997; Xia et al. 2003), suggesting that λN or the λN:*nutBoxB* complex might simply displace NusA(431–490) in the competition for the RNA-binding site. This is in accordance with the complex-stabilizing function of the NusA(353–416)–λN(34–40) interaction.

To get further insight into the role of NusA(353–416) and NusA(431–490) in termination and anti-termination, our future research will focus on the elucidation of the complexes of NusACTD with λN and αCTD, as well as investigation of the intramolecular interaction of NusA(431–490) and the RNA-binding sites of NusA.

Materials and methods

Protein production

λN(1–53) was expressed in *E. coli* BL21(DE3) using the pTKK19 expression vector (Kohno et al. 1998). The resulting fusion protein consisted of an amino-terminal deca-histidine-tag, followed by ubiquitin and λN(1–53), and was purified by immobilized nickel-affinity chromatography under nonnative conditions. Subsequent cleavage by yeast ubiquitin hydrolase and a further high-performance liquid chromatography step yielded pure λN(1–53). *E. coli* αCTD(233–329) was expressed as a deca-histidine-tagged protein in BL21(DE3) from pET-19b (Novagen) and purified by immobilized nickel-affinity chromatography under native conditions. The histidine-tag was cleaved off with rhinovirus protease 3C (Cordingley et al. 1990), resulting in two additional amino-terminal residues (Gly-Pro). NusACTD was expressed and purified as GP-NusA(339–495) (Eisenmann et al. 2004). NMR samples contained 0.5–1.5 mM GP-NusA(339–495) in 10 mM potassium phosphate (pH 6.8), 50 mM sodium chloride, 0.02% sodium azide, and 10% D_2O.

NMR spectroscopy

All NMR experiments were performed at 298 K on Bruker Avance400, DRX600, Avance700, and Avance800 spectrometers equipped with inverse $^1H/^{13}C/^{15}N$ triple-resonance probes with pulsed-field gradient capabilities. In addition to the spectra needed for backbone and side-chain resonance assignments (Eisenmann et al. 2004), ^{13}C-NOESY-HSQC, ^{15}N-NOESY-HSQC, CNH-NOESY, CCH-NOESY, NNH-NOESY, and 4D-C,C-NOESY experiments with mixing times of 120 msec were acquired on uniformly ^{15}N and ^{15}N, ^{13}C-labeled GP-NusA(339–495) at a concentration of 1.5 mM to obtain distance restraints (Sattler et al. 1999). For angle restraints, $^3J(H^N H^A)$ scalar coupling constants were determined from intensity ratios of diagonal and cross-peaks in the HNHA spectrum (Vuister and Bax 1993). Slowly exchanging amide protons were identified in a series of ^{15}N-HSQC spectra acquired after dissolving freeze-dried ^{15}N-labeled GP-NusA(339–495) in D_2O, and those amide protons still visible after 15 min were assumed to be involved in hydrogen bonds. $^1D(NH^N)$ RDCs were obtained from J-modulated HSQC experiments at 800 MHz (Tjandra et al. 1996) with a 0.5-mM sample of GP-NusA(339–495) in the presence of 10 mg/mL Pf1 phage (Hansen et al. 1998) by subtracting the $^1J(NH^N)$ scalar coupling constants measured in reference spectra without Pf1 phage. A sample of 0.5 mM ^{15}N-labeled GP-NusA(339–495) was used for measuring ^{15}N R_1 and R_2 rates, as well as the HetNOE, with published pulse sequences (Dayie and Wagner 1994). For the determination of R_1 and R_2 at a proton frequency of 600 MHz, spectra were recorded with delays of 6.88 (3×), 752.33 (3×), 1020.48 (3×), and 1288.63 (3×) msec, and 16.96 (3×), 84.4 (3×), 101.76 (3×), and 118.72 (3×) msec, respectively.

The HetNOEs were averaged over two independent data sets. The NMR data were processed using NMRPipe (Delaglio et al. 1995) and in-house written software, and analyzed with the program package NMRview5.0.4 (Johnson and Blevins 1994). Diffusion experiments were performed at a proton resonance frequency of 400 MHz on samples of 175, 350, and 700 μM GP-NusA(339–495) in D_2O containing 0.5% dioxan, 10 mM potassium phosphate (pH 6.8), 50 mM sodium chloride, and 0.02% sodium azide. For each experiment, five independent series of 1D spectra were acquired using the PG-SLED pulse sequence (Jones et al. 1997) with a gradient time of 7 msec, an echo time of 70 msec, and gradient strengths of 5%–50% in 5% increments, and 50%–100% in 6.25% increments. A single Gaussian was fitted to the decay of the protein signal, and the decay of the dioxane signal was described by two Gaussians to account for the overlap of the dioxane signal with the protein signal. Titrations were performed by adding aliquots of a concentrated stock solution of unlabeled λN(1–53) or αCTD(233–329) to a sample of ~0.5 mM ^{15}N-labeled GP-NusA(339–495) and acquiring ^{1}H^{15}N HSQC spectra at 700 MHz after each titration step. In both titrations, ligands were added to GP-NusA(339–495) until no further changes could be observed in the spectra.

Structure calculation

Distance restraints for structure calculation were derived from NNH-NOESY, ^{13}C- and ^{15}N-NOESY-HSQC spectra, and 4D-C,C-NOESY spectra. NOESY cross-peaks were classified according to their relative intensities and converted to distance restraints with upper limits of 2.7 Å (strong), 3.5 Å (medium), and 5.0 Å (weak). For ambiguous distance restraints, the r^{-6} summation over all assigned possibilities defined the upper limit (Nilges 1995).

The raw scalar coupling constants were multiplied with a correction factor of 1.1 to take into account the different relaxation rates of in-phase and anti-phase components (Vuister and Bax 1993). Residues with scalar coupling constants below 6 Hz were restrained to dihedral angles between −80° and −40°, residues showing coupling constants above 8 Hz were restricted to dihedral angles of −160° to −80° (Schweimer et al. 2002). Glycines were omitted, since they were not stereospecifically assigned, and since the coupling constants are likely affected by cross-relaxation (Vuister and Bax 1993).

Hydrogen bonds were included in the final structure calculation if the acceptor of a slowly exchanging amide proton could be identified from the results of preceding structure calculations. Thus, a hydrogen bond was assumed if the distance of the carboxyl oxygen and the amide proton was below 2.6 Å, and the angle of the amide proton, the amide nitrogen, and the carboxyl oxygen was $< 60°$ in all accepted structures. For each hydrogen bond, the distance between the amide proton and the acceptor was restrained to < 2.3 Å, and the distance between the amide nitrogen and the acceptor was restrained to < 3.3 Å (Schweimer et al. 2002).

All prolines were considered to adopt the *trans* conformation as strong $H^A(i)$-$H^D(i+1)$ and $H^N(i)$ and $H^D(i+1)$ NOEs could be observed (Wüthrich 1986).

The structures for NusA(351–426) and NusA(426–495) were calculated separately, since no NOEs could be observed between the two regions, and relaxation data suggested an at least partly independent reorientation of the two regions. GP-NusA(339–350) was omitted in the structure calculation, due to the lack of inter-residual NOEs and low values of the HetNOEs, both indicating a flexible amino terminus.

The structure calculations were performed with the program XPLOR-NIH 1.2.1 (Schwieters et al. 2003) using a three-step simulated annealing protocol (Nilges et al. 1988a,b,c) with floating assignment of prochiral groups (Folmer et al. 1997).

First conformational space, sampling was carried out for 120 psec with a time step of 3 fsec at a temperature of 2000 K, followed by a cooling period of 120 psec down to 1000 K, and 60 psec cooling to 100 K, both with a time step of 2 fsec. A modified conformational database potential for backbone and side-chain dihedral angles was applied (Kuszewski and Clore 2000; Neudecker et al. 2001). The proline angles were modified according to Neudecker et al. (2004). After simulated annealing, the structures were subjected to 1000 steps of Powell minimization (Powell 1977), and the final 500 steps were minimized without conformational database potential.

In a first step, 90 structures were calculated (Table 1) using 883/699 [NusA(351–426)/NusA(426–495)] distance and 39/28 dihedral angle restraints; in a second step, 38/40 additional restraints from hydrogen exchange experiments were included. The 32 structures with the lowest total energy were then refined using 37/32 ^{1}D(NH^N) RDCs with a harmonic potential (Tjandra et al. 1997). Flexible residues (for definition, see "NMR data relaxation analysis," below) were excluded from the calculations. The tensor components of the alignment were optimized separately for NusA(351–426) and NusA(426–495) with a grid search by varying the axial component D_a and the rhombicity R in steps of 0.5 and 0.1, respectively. The initial values of D_a and R were estimated from the distribution of the ^{1}D(NH^N) (Clore et al. 1998) and a molecular dynamics run was performed for each pair of D_a and R, yielding axial components of 10.5 ± 0.25 Hz [NusA(351–426)] and 6.5 ± 0.25 Hz [NusA(426–495)], and rhombicities of 0.2 ± 0.05 [NusA(351–426)] and 0.3 ± 0.05 [NusA(426–495)] for the energetically most favorable combination of D_a and R.

The 19 structures showing the lowest values of the target function excluding the database potential were further analyzed with XPLOR-NIH 1.2.1 (Schwieters et al. 2003) and PROCHECK 3.5.4 (Morris et al. 1992; Laskowski et al. 1993).

Helix angles in the average structure were estimated by interpolating axes through all heavy atoms in each of the helices according to the MOLMOL least-squares algorithm.

NMR relaxation data analysis

Relaxation rates were calculated by least-squares fitting of mono-exponential decays to the peak-heights with the program Curvefit (A.G. Palmer III, Columbia University, NY, unpubl.). Errors were estimated to be 5% for relaxation rates and 10% for the HetNOEs. The coarse filter of Pawley et al. (2001) served to identify flexible residues [six in NusA(353–416), 12 in NusA(431–490)], that is, residues with significant motions on a pico- to nanosecond timescale, and residues probably involved in exchange processes. Additionally, residues outside of regular secondary structure and H353, Y362, L373, and Y386 were not taken into account for the calculation of the diffusion tensors with Tensor2 (Dosset et al. 2000) using standard settings. Hydrodynamic parameters of an elongated NusA(353–490) molecule were computed with HYDRONMR version 5a using a shell model (de la Torre and Carrasco 2000).

References

Atkinson, A.R. and Kieffer, B. 2004. The role of protein motions in molecular recognition: Insights from heteronuclear NMR relaxation measurements. *Prog. Nucl. Magn. Reson. Spectrosc.* **44:** 141–187.

Bax, A., Kontaxis, G., and Tjandra, N. 2001. Dipolar couplings in macro-molecular structure determination. *Methods Enzymol.* **339:** 127–174.

Berman, H.M., Westbrook, J., Feng, Z., Gilliland, G., Bhat, T.N., Weissig, H., Shindyalov, I.N., and Bourne, P.E. 2000. The Protein Data Bank. *Nucleic Acids Res.* **28:** 235–242.

Bonin, I., Muhlberger, R., Bourenkov, G.P., Huber, R., Bacher, A., Richter, G., and Wahl, M.C. 2004. Structural basis for the interaction of *Escherichia coli* NusA with protein N of phage λ. *Proc. Natl. Acad. Sci.* **101:** 13762–13767.

Braddock, D.T., Cai, M., Baber, J.L., Huang, Y., and Clore, G.M. 2001. Rapid identification of medium- to large-scale interdomain motion in modular proteins using dipolar couplings. *J. Am. Chem. Soc.* **123:** 8634–8635.

Braddock, D.T., Louis, J.M., Baber, J.L., Levens, D., and Clore, G.M. 2002. Structure and dynamics of KH domains from FBP bound to single-stranded DNA. *Nature* **415:** 1051–1056.

Clore, G.M., Gronenborn, A.M., and Bax, A. 1998. A robust method for determining the magnitude of the fully asymmetric alignment tensor of oriented macromolecules in the absence of structural information. *J. Magn. Reson.* **133:** 216–221.

Cordingley, M.G., Callahan, P.L., Sardana, V.V., Garsky, V.M., and Colonno, R.J. 1990. Substrate requirements of human rhinovirus 3C protease for peptide cleavage *in vitro*. *J. Biol. Chem.* **265:** 9062–9065.

Dayie, K.T. and Wagner, G. 1994. Relaxation-rate measurements for [15]N-^{1}H groups with pulsed-field gradients and preservation of coherence pathways. *J. Magn. Reson.* **111A:** 121–126.

Delaglio, F., Grzesiek, S., Vuister, G.W., Zhu, G., Pfeifer, J., and Bax, A. 1995. NMRPipe: A multidimensional spectral processing system based on UNIX pipes. *J. Biomol. NMR* **6:** 277–293.

de la Torre, J. and Carrasco, H.B. 2000. HYDRONMR: Prediction of NMR relaxation of globular proteins from atomic level structures and hydrodynamic calculations. *J. Magn. Reson.* **147B:** 138–146.

Doherty, A.J., Serpell, L.C., and Ponting, C.P. 1996. The helix-hairpin-helix DNA-binding motif: A structural basis for non-sequence-specific recognition of DNA. *Nucleic Acids Res.* **24:** 2488–2497.

Dosset, P., Hus, J.C., Blackledge, M., and Marion, D. 2000. Efficient analysis of macromolecular rotational diffusion from heteronuclear relaxation data. *J. Biomol. NMR* **16:** 23–28.

Eisenmann, A., Schwarz, S., Rösch, P., and Schweimer, K. 2004. Sequence-specific ^{1}H, ^{13}C, ^{15}N resonance assignments and secondary structure of the carboxy-terminal domain of the *E. coli* transcription factor NusA. *J. Biomol. NMR* **28:** 193–194.

Folmer, R.H., Hilbers, C.W., Konings, R.N., and Nilges, M. 1997. Floating stereospecific assignment revisited: Application to an 18 kDa protein and comparison with J-coupling data. *J. Biomol. NMR* **9:** 245–258.

Fushman, D., Varadan, R., Assfalg, M., and Walker, O. 2004. Determining domain orientation in macromolecules by using spin-relaxation and residual dipolar coupling measurements. *Prog. Nucl. Magn. Reson. Spectrosc.* **44:** 189–214.

Gopal, B., Haire, L.F., Gamblin, S.J., Dodson, E.J., Lane, A.N., Papavinasasundaram, K.G., Colston, M.J., and Dodson, G. 2001. Crystal structure of the transcription elongation/anti-termination factor NusA from *Mycobacterium tuberculosis* at 1.7 Å resolution. *J. Mol. Biol.* **314:** 1087–1095.

Gusarov, I. and Nudler, E. 2001. Control of intrinsic transcription termination by N and NusA: The basic mechanisms. *Cell* **107:** 437–449.

Hansen, M.R., Mueller, L., and Pardi, A. 1998. Tunable alignment of macromolecules by filamentous phage yields dipolar coupling interactions. *Nat. Struct. Biol.* **5:** 1065–1074.

Holm, L. and Sander, C. 1996. Mapping the protein universe. *Science* **273:** 595–602.

Johnson, B.A. and Blevins, R.A. 1994. NMRview: A computer program for the visualization and analysis of NMR data. *J. Biomol. NMR* **4:** 603–614.

Jones, J.A., Wilkins, D.K., Smith, L.J., and Dobson, C.M. 1997. Characterisation of protein unfolding by NMR diffusion measurements. *J. Biomol. NMR* **10:** 199–203.

Kay, L.E., Torchia, D.A., and Bax, A. 1989. Backbone dynamics of proteins as studied by ^{15}N inverse detected heteronuclear NMR spectroscopy: Application to staphylococcal nuclease. *Biochemistry* **28:** 8972–8979.

Kim, C.A. and Bowie, J.U. 2003. SAM domains: Uniform structure, diversity of function. *Trends Biochem. Sci.* **28:** 625–628.

Kohno, T., Kusunoki, H., Sato, K., and Wakamatsu, K. 1998. A new general method for the biosynthesis of stable isotope-enriched peptides using a decahistidine-tagged ubiquitin fusion system: An application to the production of mastoparan-X uniformly enriched with ^{15}N and ^{15}N/[13]C. *J. Biomol. NMR* **12:** 109–121.

Koradi, R., Billeter, M., and Wüthrich, K. 1996. MOLMOL: A program for display and analysis of macromolecular structure. *J. Mol. Graph.* **14:** 51–55.

Kumar, S. and Bansal, M. 1998. Dissecting α-helices: Position specific analysis of α-helices in globular proteins. *Proteins* **31:** 460–476.

Kuszewski, J. and Clore, G.M. 2000. Sources of and solution to problems in the refinement of protein NMR structures against torsion angle potentials of mean force. *J. Magn. Reson.* **146:** 249–254.

Laskowski, R.A., MacArthur, M.W., Moss, D.S., and Thornton, J.M. 1993. PROCHECK: A program to check the stereochemical quality of protein structures. *J. Appl. Cryst.* **26:** 283–291.

Liu, K., Zhang, Y., Severinov, K., Das, A., and Hanna, M.M. 1996. Role of *Escherichia coli* RNA polymerase α subunit in modulation of pausing, termination, and antitermination by the transcription elongation factor NusA. *EMBO J.* **15:** 150–161.

Maciejewski, M.W., Liu, D., Prasad, R., Wilson, S.H., and Mullen, G.P. 2000. Backbone dynamics and refined solution structure of the N-terminal domain of DNA polymerase β. Correlation with DNA binding and dRP lyase activity. *J. Mol. Biol.* **296:** 229–253.

Mah, T.F., Li, J., Davidson, A.R., and Greenblatt, J. 1999. Functional importance of regions in *Escherichia coli* elongation factor NusA that interact with RNA polymerase, the bacteriophage λ N protein and RNA. *Mol. Microbiol.* **34:** 523–537.

Mah, T.F., Kuznedelov, K., Mushegian, A., Severinov, K., and Greenblatt, J. 2000. The α subunit of *E. coli* RNA polymerase activates RNA binding by NusA. *Genes & Dev.* **14:** 2664–2675.

Mandel, A.M., Akke, M., and Palmer, A.G. 1995. Backbone dynamics of *Escherichia coli* ribonuclease HI: Correlations with structure and function in an active enzyme. *J. Mol. Biol.* **246:** 144–163.

Mogridge, J., Mah, T.F., and Greenblatt, J. 1995. A protein-RNA interaction network facilitates the template-independent cooperative assembly on RNA polymerase of a stable antitermination complex containing the λ N protein. *Genes & Dev.* **9:** 2831–2845.

Mogridge, J., Legault, P., Li, J., Van Oene, M.D., Kay, L.E., and Greenblatt, J. 1998. Independent ligand-induced folding of the RNA-binding domain and two functionally distinct antitermination regions in the phage λ N protein. *Mol. Cell* **1:** 265–275.

Mooney, R.A., Artsimovitch, I., and Landick, R. 1998. Information processing by RNA polymerase: Recognition of regulatory signals during RNA chain elongation. *J. Bacteriol.* **180:** 3265–3275.

Morris, A.L., MacArthur, M.W., Hutchinson, E.G., and Thornton, J.M. 1992. Stereochemical quality of protein structure coordinates. *Proteins* **12:** 345–364.

Neudecker, P., Sticht, H., and Rösch, P. 2001. Improving the efficiency of the Gaussian conformational database potential for the refinement of protein and nucleic acid structures. *J. Biomol. NMR* **21:** 373–375.

Neudecker, P., Nerkamp, J., Eisenmann, A., Nourse, A., Lauber, T., Schweimer, K., Lehmann, K., Schwarzinger, S., Ferreira, F., and Rösch, P. 2004. Solution structure, dynamics, and hydrodynamics of the calcium-bound cross-reactive birch pollen allergen Bet v 4 reveal a canonical monomeric two EF-hand assembly with a regulatory function. *J. Mol. Biol.* **336:** 1141–1157.

Nilges, M. 1995. Calculation of protein structures with ambiguous distance restraints. Automated assignment of ambiguous NOE crosspeaks and disulfide connectivities. *J. Mol. Biol.* **245:** 645–660.

Nilges, M., Clore, G.M., and Gronenborn, A.M. 1988a. Determination of three-dimensional structures of proteins from interproton distance data by hybrid distance geometry-dynamical simulated annealing calculations. *FEBS Lett.* **229:** 317–324.

———. 1988b. Determination of three-dimensional structures of proteins from interproton distance data by dynamical simulated annealing from a random array of atoms. Circumventing problems associated with folding. *FEBS Lett.* **239:** 129–136.

Nilges, M., Gronenborn, A.M., Brunger, A.T., and Clore, G.M. 1988c. Determination of three-dimensional structures of proteins by simulated annealing with interproton distance restraints. Application to crambin, potato carboxypeptidase inhibitor, and barley serine proteinase inhibitor 2. *Protein Eng.* **2:** 27–38.

Notredame, C., Higgins, D., and Heringa, J. 2000. T-Coffee: A novel method for multiple sequence alignments. *J. Mol. Biol.* **302:** 205–217.

Nudler, E. 1999. Transcription elongation: Structural basis and mechanisms. *J. Mol. Biol.* **288:** 1–12.

Nudler, E. and Gottesman, M.E. 2002. Transcription termination and antitermination in *E. coli. Genes Cells* **7:** 755–768.

Pawley, N.H., Wang, C., Koide, S., and Nicholson, L.K. 2001. An improved method for distinguishing between anisotropic tumbling and chemical exchange in analysis of ^{15}N relaxation parameters. *J. Biomol. NMR.* **20:** 149–165.

Powell, M.J.D. 1977. Restart procedures for the conjugate gradient method. *Math. Progr.* **12:** 241–254.

Sattler, M., Schleucher, J., and Griesinger, C. 1999. Heteronuclear multi-dimensional NMR experiments for the structure determination of proteins in solution employing pulsed field gradients. *Prog. Nucl. Magn. Reson. Spectrosc.* **34:** 39–158.

Schweimer, K., Hoffmann, S., Bauer, F., Friedrich, U., Kardinal, C., Feller, S.M., Biesinger, B., and Sticht, H. 2002. Structural investigation of the binding of a herpesviral protein to the SH3 domain of tyrosine kinase Lck. *Biochemistry* **41:** 5120–5130.

Schwieters, C.D., Kuszewski, J.J., Tjandra, N., and Clore, G.M. 2003. The Xplor-NIH NMR molecular structure determination package. *J. Magn. Reson.* **160:** 66–74.

Shao, X. and Grishin, N.V. 2000. Common fold in helix-hairpin-helix proteins. *Nucleic Acids Res.* **28:** 2643–2650.

Shin, D.H., Nguyen, H.H., Jancarik, J., Yokota, H., Kim, R., and Kim, S.H. 2003. Crystal structure of NusA from *Thermotoga maritima* and functional implication of the N-terminal domain. *Biochemistry* **42:** 13429–13437.

Stevens, S.Y., Sanker, S., Kent, C., and Zuiderweg, E.R. 2001. Delineation of the allosteric mechanism of a cytidylyltransferase exhibiting negative cooperativity. *Nat. Struct. Biol.* **8:** 947–952.

Thanos, C.D., Faham, S., Goodwill, K.E., Cascio, D., Phillips, M., and Bowie, J.U. 1999. Monomeric structure of the human EphB2 sterile α motif domain. *J. Biol. Chem.* **274:** 37301–37306.

Tjandra, N., Feller, S.E., Pastor, R.W., and Bax, A. 1995. Rotational diffusion anisotropy of human ubiquitin from ^{15}N relaxation. *J. Am. Chem. Soc.* **117:** 12562–12566.

Tjandra, N., Grzesiek, S., and Bax, A. 1996. Magnetic field dependence of nitrogen-proton J splittings in ^{15}N-enriched human ubiquitin resulting from relaxation interference and residual dipolar coupling. *J. Am. Chem. Soc.* **118:** 6264–6272.

Tjandra, N., Omichinski, J.G., Gronenborn, A.M., Clore, G.M., and Bax, A. 1997. Use of dipolar ^{1}H-^{15}N and ^{1}H-^{13}C couplings in the structure determination of magnetically oriented macromolecules in solution. *Nat. Struct. Biol.* **4:** 732–738.

Tsugawa, A., Saito, M., Court, D.L., and Nakamura, Y. 1988. NusA amber mutation that causes temperature-sensitive growth of *Escherichia coli. J. Bacteriol.* **170:** 908–915.

van Gilst, M.R. and von Hippel, P.H. 1997. Assembly of the N-dependent antitermination complex of phage λ. NusA and RNA bind independently to different unfolded domains of the N protein. *J. Mol. Biol.* **274:** 160–173.

Vuister, W.G. and Bax, A. 1993. Quantitative J correlation: A new approach for measuring homonuclear three-bond J(H^{N}H^{A}) coupling constants in ^{15}N-enriched proteins. *J. Am. Chem. Soc.* **115:** 7772–7777.

Wilkins, D.K., Grimshaw, S.B., Receveur, V., Dobson, C.M., Jones, J.A., and Smith, L.J. 1999. Hydrodynamic radii of native and denatured proteins measured by pulse field gradient NMR techniques. *Biochemistry* **38:** 16424–16431.

Worbs, M., Bourenkov, G.P, Bartunik, H.D., Huber, R., and Wahl, M.C. 2001. An extended RNA binding surface through arrayed S1 and KH domains in transcription factor NusA. *Mol. Cell.* **7:** 1177–11789.

Wüthrich, K. 1986. *NMR of proteins and nucleic acids.* Wiley, New York.

Xia, T., Frankel, A., Takahashi, T.T., Ren, J., and Roberts, R.W. 2003. Context and conformation dictate function of a transcription antitermination switch. *Nat. Struct. Biol.* **10:** 812–819.

Zuiderweg, E.R. 2002. Mapping protein-protein interactions in solution by NMR spectroscopy. *Biochemistry* **41:** 1–7.